Activity-dependent lateral inhibition enables ensemble synchronization of odor-activated neurons in the olfactory bulb

Tal Dalal, Rafi Haddad*

The Gonda Multidisciplinary Brain Research Center, Bar-Ilan University, Ramat-Gan, 5290002, Israel.

*Author for correspondence: rafi.haddad@biu.ac.il

Abstract

Information in the brain is represented by the activity of neuronal ensembles. These ensembles are adaptive and dynamic, formed and truncated based on the animal`s experience. One mechanism by which spatially distributed neurons form an ensemble is synchronizing their spiking activity in response to a sensory event. In the olfactory bulb, odor stimulation evokes rhythmic gamma activity in spatially distributed mitral and tufted cells (MTCs). This rhythmic activity is thought to enhance the relay of odor information to the downstream olfactory targets. However, how only the odor-activated MTCs are synchronized is unknown. Here, we demonstrate that light activating one set of MTCs can gamma-entrain the spiking activity of another set. This lateral synchronization was particularly effective when both MTCs fired at the gamma rhythm, facilitating the synchronization of only the odor-activated MTCs. Furthermore, we show that lateral synchronization did not depend on the distance between the MTCs and is mediated by Granule cells. In contrast, lateral inhibition between MTCs that reduced their firing rates was spatially restricted to adjacent MTCs and was not mediated by Granule cells. Our findings reveal a simple yet robust mechanism by which spatially distributed neurons entrain each other's spiking activity to form an ensemble.

Highlights

1) MTC activation entrains the spike timing of other MTCs in an activity-dependent and spatially-independent manner.
2) MTC to MTC suppression is activity- and distance-dependent
3) Spatially distributed Granule cells control MTC's spike timing, yet do not substantially affect their firing rate.

Introduction

Information in the brain is represented by the activity of ensembles of neurons, typically interconnected through a network of interneurons (Buzsáki and Chrobak, 1995). These interactions reshape the ensemble activity as it evolves in time and space. One mechanism by which spatially distributed neurons form an ensemble is by synchronizing their spiking activity in response to a sensory event (Buzsáki, 2010). This synchronization is thought to enhance the transmission of information to downstream targets (Dalal and Haddad, 2022; Macleod et al., 1998; Pritchett et al., 2015; Sohal, 2016).

The olfactory bulb (OB) is the first processing station of the olfactory system. In the OB, odors are represented by sets of activated glomeruli that reflect the responses of olfactory sensory neurons. Each glomerulus innervates a small number of MTCs. These MTCs interact with each other via a dense network of inhibitory neurons stratified throughout all six OB layers. Several studies have shown that odorants evoke strong spike gamma-entrainment in MTCs (Beshel et al., 2007; Dalal and Haddad, 2022; Fukunaga et al., 2014; Lepousez and Lledo, 2013), as well as synchronous firing of MTCs (Kashiwadani et al., 1999). This synchronization is mediated by granule cells (Schoppa, 2006)(GCs) and has recently been shown to enhance odor-information transmission to the Piriform cortex (Dalal and Haddad, 2022). However, the method by which only the odor-activated MTCs are synchronized is unknown. One prominent hypothesis is that GCs enable synchronization solely between odor-activated MTCs (Egger and Kuner, 2021; Galán et al., 2006).

GCs are the most abundant type of interneuron in the OB. They form dendrodendritic synapses with MTCs (Shepherd, 2004) and, via these synapses, can provide recurrent and long-range lateral inhibition. Earlier studies suggested that GCs mediate lateral inhibition between MTCs shaping their firing rate (Arevian et al., 2008; Giridhar et al., 2011; Yokoi et al., 1995). In contrast, more recent studies demonstrated that in-vivo lateral inhibition is sparse and weak (Fantana et al., 2008; Lehmann et al., 2016; Pressler and Strowbridge, 2017), therefore unlikely to substantially suppress MTC firing rates. One study showed that optogenetically silencing the GCs did not affect odor-evoked

63 inhibitory responses (Fukunaga et al., 2014). These findings cast doubts on the role of GCs
64 in suppressing MTCs' odor-evoked firing rate (Burton, 2017).
65 Here, we used odor and optogenetic stimulations of MTCs and GCs in anesthetized
66 mice, to study how active MTC ensembles interact to regulate their spikes' timing and
67 firing rates. We found that MTCs form two types of interactions that are mediated by two
68 types of interneurons. One interaction enables the synchronization of only odor-activated
69 MTCs dispersed on the OB surface, and is mediated by GCs. The other type of interaction
70 affecting MTC firing rate is limited to relatively nearby MTCs, and, contrary to the view
71 in the field, is *not* mediated by GCs.
72
73 **Results**
74 **Activity-Dependent Lateral Synchronization of MTCs**
75 To investigate how MTCs interact we expressed the light-gated channel rhodopsin (ChR2)
76 exclusively in MTCs by crossing the Tbet-Cre and Ai39 mice lines (Grobman et al., 2018;
77 Haddad et al., 2013), and recorded the spiking activity of MTCs in anesthetized mice
78 during optogenetic stimulation. We first mapped each recorded cell's receptive field, i.e.,
79 the glomeruli on the dorsal OB that affect its firing rates when they are light-stimulated.
80 Pseudo-random light patterns composed of multiple light spots were projected over the OB
81 surface (Supplementary Figure 1a) and the spike-triggered-average was computed to obtain
82 the receptive field map (Figure 1a; 'STA', see Methods). Each light pattern comprised 5-
83 10 multiple light spots of size 88-110 μm^2. This stimulation protocol ensured the activation
84 of varied MTC combinations associated with different glomeruli, among them the MTC
85 we recorded from. As expected, light-stimulating the area above the recording electrode
86 activated the recorded MTC (the 'hotspot'). This protocol also revealed regions on the OB
87 surface that had a suppressive effect on the activity of the recorded MTC (Figure 1a). Based
88 on the receptive field map, we selected several spots and light-activated them either alone
89 or simultaneously with the spot that activated the recorded MTC using four increasing light
90 intensities (Figure 1a-b; N = 5 mice; 27 neurons; overall 127 pairs were tested, 2-8 different
91 pairs per cell). We found that in a subset of neurons, paired light activation precisely
92 aligned the spike times of the recorded MTC across and within trials without affecting its
93 firing rate (Figure 1c and Supplementary Figure 1b), giving rise to a gamma rhythm (Figure

1d-e and Supplementary Figure 1c). To quantify the change in spike precision and gamma entrainment at the population level, we computed the difference in the area under the power spectrum density (PSD) curve between the two conditions at the gamma range (termed as 'delta entrainment'; 40-70Hz, see Methods). We found that the change in entrainment was significantly higher than zero (Figure 1f; $P < 0.001$ and $P = 0.13$ for real and shuffled data, respectively; two-tailed paired *t*-test, N = 319/511 values from all pairs and light intensities that significantly responded to light stimulation). Overall, we found that in ~16% of the stimulated pairs, paired activation significantly enhanced the gamma entrainment (N = 50/319 delta values that exceeded the 95% confidence interval of the shuffled distribution, colored brown in Figure 1f). Varying the light intensities revealed that the enhanced gamma entrainment was most effective when the postsynaptic MTCs firing rate was ~40Hz (Figure 1g). Analyzing the locations in which paired activation significantly increased the temporal precision revealed no significant correlation between the pair's distance and its gamma entrainment change, suggesting that lateral entrainment is driven by MTCs distributed on the OB surface without any discernable spatial organization (Figure 1h; $r = 0.05$, $P = 0.73$, Spearman correlation). Overall, we found activity-dependent enhancement of MTC spike precision in the gamma range that is distance-independent.

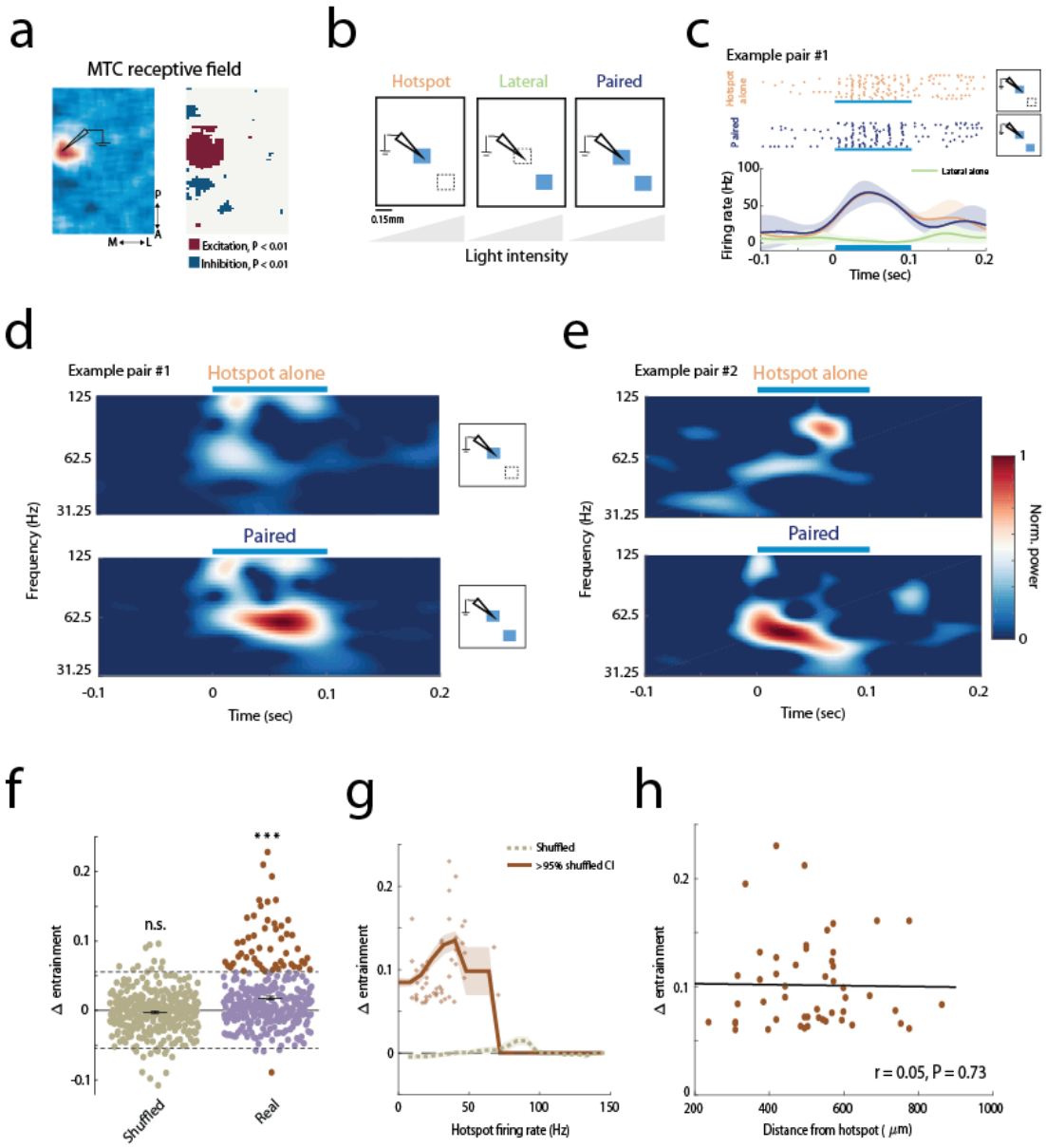

Figure 1: Activity-dependent lateral-enhancement of spike times

a) Left: STA map with an excitatory region near the electrode location and presumably several surrounding inhibitory spots. Right: the significance map ($P < 0.01$ relative to shuffled data, see Methods).

b) Schematic illustration of the experimental setups. Photo-stimulation of each spot alone (hotspot or lateral spot conditions marked by orange and green text, respectively) or paired stimulation (marked in blue) using four different light intensities.

c) Raster plots and smoothed PSTHs of the response to light stimulation of the hotspot (top, orange) and paired stimulation (middle, blue). Note, the increase in spike time accuracy within and across trials when both spots are activated (middle panel). Light stimulation did not affect the average firing rate (lower panel). The effect of light stimulation of the lateral spot alone is shown in green.

d-e) Examples of MTCs time-frequency wavelet analysis from two different mice. Example pair #1 is the pair displayed in **c**. Both examples show a strong gamma rhythm following paired stimulation. In pair #1, gamma power peaked at ~58Hz, and pair #2 at ~48Hz.

f) Paired stimulation increased the spikes' temporal precision. Mean ± SEM of the change in spikes entrainment at the population level (N = 319/511 values from all pairs and light intensities that significantly responded to light stimulation, P = 0.13 and P < 0.001 for shuffled (green) and real (purple) data, respectively; two-tailed paired *t*-test). In brown are values that exceeded the 95% confidence interval of the shuffled data distribution values of increased and decreased spike entrainment, respectively; confidence interval is marked by dashed black lines).

g) Lateral entrainment is activity-dependent. The moving average of the data shown in f is plotted as a function of the firing rate of the postsynaptic MTC (N = 50 values of increased entrainment). The increase in entrainment was largest when the neuron fired at ~40Hz. The color code is the same as in **f**. The shuffled data is shown in a dashed green line.

h) Spike entrainment does not depend on the distance between the MTC pair. No significant correlation was found between the increase in spike-entrainment and the distance from the hotspot (r = 0.05, P = 0.73, Spearman correlation; N = 50 values with significant increase in spike entrainment, brown dots in **g**).

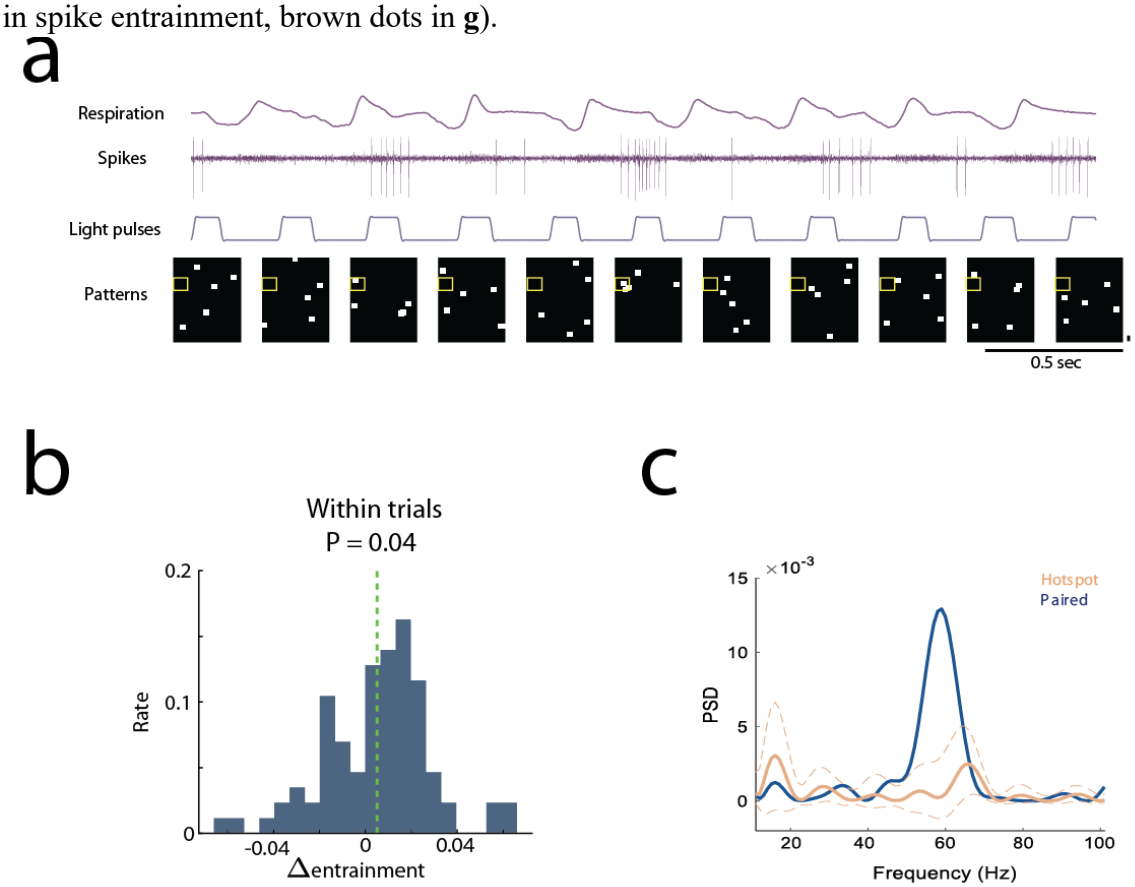

Supplementary Figure 1: Spike entrainment between and within trials

a) Light stimulation protocol. An image containing N randomly distributed light patches (N = 5 in this example) is projected on the dorsal bulb in each trial. The light patterns

are shown in the bottom panel. The yellow rectangle marks the region around the recording electrode. The spiking activity and the respiratory signal are shown above. Multiplying each pattern by the firing rate it evoked and averaging across all trials gives the STA activity map (see Methods). Scale bars: 0.5 second; 110 µm.

b) Paired activation enhances the spike precision at the gamma range within each trial (P = 0.04, two-tailed paired *t*-test, see Methods). Delta entrainment was computed per trial (see Methods). The mean is marked with a dashed green line.

c) Power spectral density (PSD) during the light stimulation duration (100 ms) of the example shown in Figure **1c-d**. Dashed lines represent the 95% confidence interval constructed using bootstrapping.

Activity-Dependent Lateral Suppression of MTCs is Confined in Space

In addition to lateral synchronization between co-active MTCs, we found that paired activation could suppress the recorded MTC firing rate (Figure 2a-b). Figure 2c shows the response of a recorded MTC when light-stimulated alone, and simultaneously with other MTCs under four different light intensities (pair #1 or pair #2, as marked in Figure 2a). Activation of pair #1 evoked lateral suppression that was dependent on the recorded MTC firing rate, while activation of pair #2 did not affect the MTC firing rate across any light intensities. Plotting the evoked change in firing rate caused by paired stimulation as a function of the MTC firing rate when stimulated alone revealed that lateral inhibition is most effective when the recorded MTC fires in the gamma range (i.e., ~30-80 Hz, Figure 2d). Light stimulating the lateral spots alone did not affect the MTC baseline firing rate (Supplementary Figure 2a). Overall, in 19% (24/127) of the tested MTC pairs, the recorded MTC was significantly inhibited following paired stimulation. In contrast to the lack of spatial organization between MTC pairs that caused spike entrainment, we found a significant correlation between the distance of the paired spots and the level of evoked inhibition (Figure 2e; r = 0.45, P = 0.001, Spearman correlation). To further verify that lateral inhibition is limited to proximal MTCs, we analyzed the inhibition found in the receptive field (STA) maps. Centering all z-scored maps relative to the 'hotspot' location (N = 27 neurons from 5 mice) revealed that MTC-to-MTC suppressive interactions are strongest and densest in regions that are adjacent to the recorded MTC (~200-400 µm) and diminished quickly beyond that (Figure 2f and Supplementary Figure 2b). Furthermore,

computing the STA maps while excluding the light patterns that contained a light spot that hit the electrode location ('hotspot' area) resulted in maps that did not contain suppressive regions (Supplementary Figure 2c-d). This analysis further confirms that lateral suppression requires the recorded MTC to be active. In summary, we show that MTC-to-MTC suppressive interactions are spatially-confined and activity-dependent.

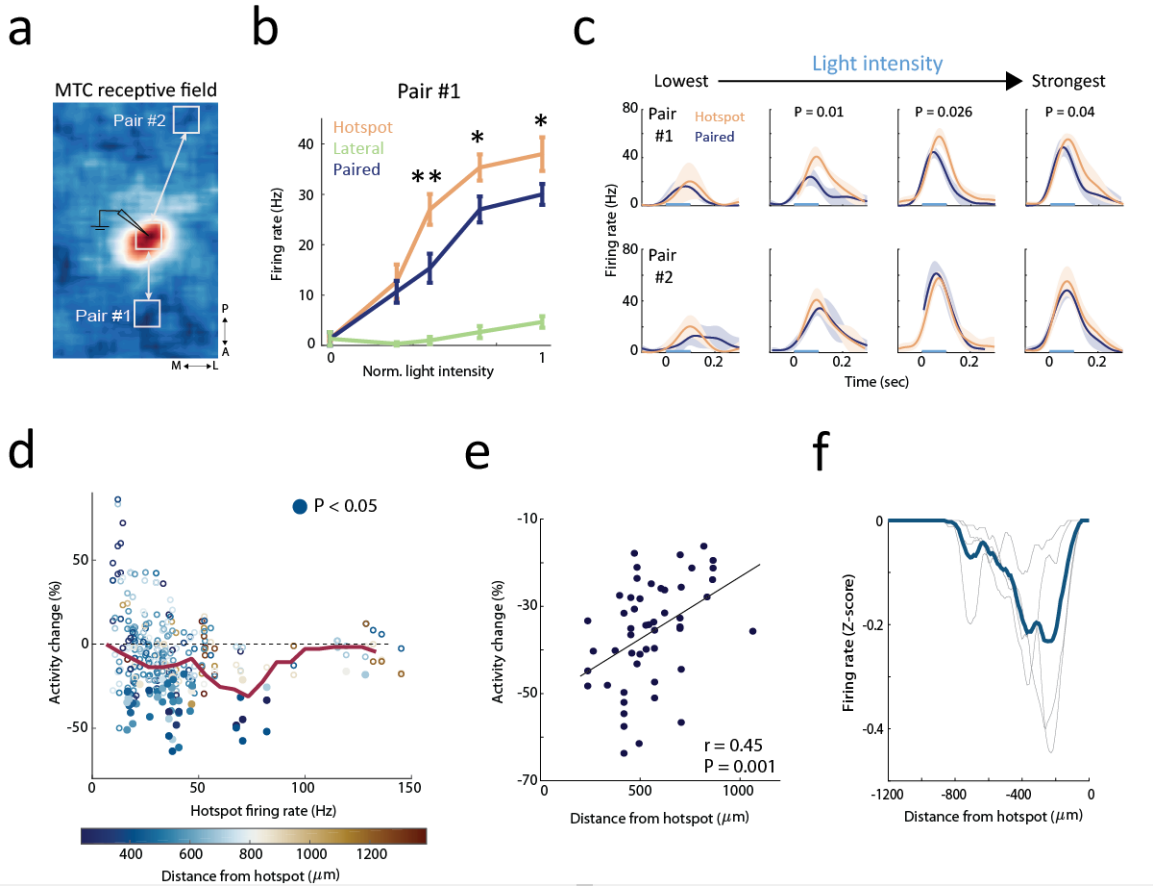

Figure 2: Activity-Dependent Lateral Suppression of MTCs is Confined in Space

a) An example of an MTC receptive field (STA map). The white rectangles mark the spots exposed to light stimulations. The hotspot location is marked with an electrode drawing.

b) Mean ± SEM firing rates of light stimulating pair #1 from **a** for each of the three conditions across all four light intensities. Activation of pair #1 (blue) caused a reduction in the recorded MTC firing rates only when the recorded MTC fired above ~25 spikes/sec. Lateral stimulation alone did not inhibit the recorded MTC (green). Zero denotes the baseline firing rate. *P < 0.05, **P < 0.01, two-tailed paired *t*-test.

c) PSTHs of pair #1 and #2 responses to light stimulations at four different light intensities. Paired stimulation of pair #1 evoked activity-dependent suppression. Paired stimulation of more distant neurons in pair #2 did not affect the recorded MTC firing rates across any tested light intensities. Light stimulation is marked

with a blue bar (0.1 sec). PSTHs without a p-value showed no significant change between the firing rates of paired stimulation and hotspot stimulation alone.

d) Summary analysis of the effect of paired activation on MTCs firing rate. Each point marks the percentage change in firing rate (Y-axis) relative to the firing rate elicited by light stimulating the hotspot alone (X-axis). Suppressive effects (i.e., negative activity change) occurred mainly when the MTC fired in the gamma range (~30-80 Hz). Color-code denotes the distance between the light-activated MTC pair. Filled circles mark significant activity change ($P < 0.05$, two-tailed unpaired *t*-test, N = 51/319 data points). The red line shows the moving average. Only light intensities that elicited a significant light response were analyzed (319/511; $P < 0.05$, two-tailed paired *t*-test).

e) Lateral suppression degrades with distance. Spearman correlation between the change in firing rate for all significant inhibitory pairs (the filled circles in **d,** N = 51) and their distance to the hotspot ($r = 0.45$, $P = 0.001$).

f) Mean firing rate of the pixels located on each of the four diagonals in the Z-scored STA maps, centered relative to the 'hotspot'. The centered map and the diagonals are shown in **Supplementary Figure 2b**. Gray lines show the response of the four sections taken from the origin towards the four corners (the four dashed lines in Supplementary Figure 2b). The blue line represents the average across all four sections. Zero denotes the hotspot location.

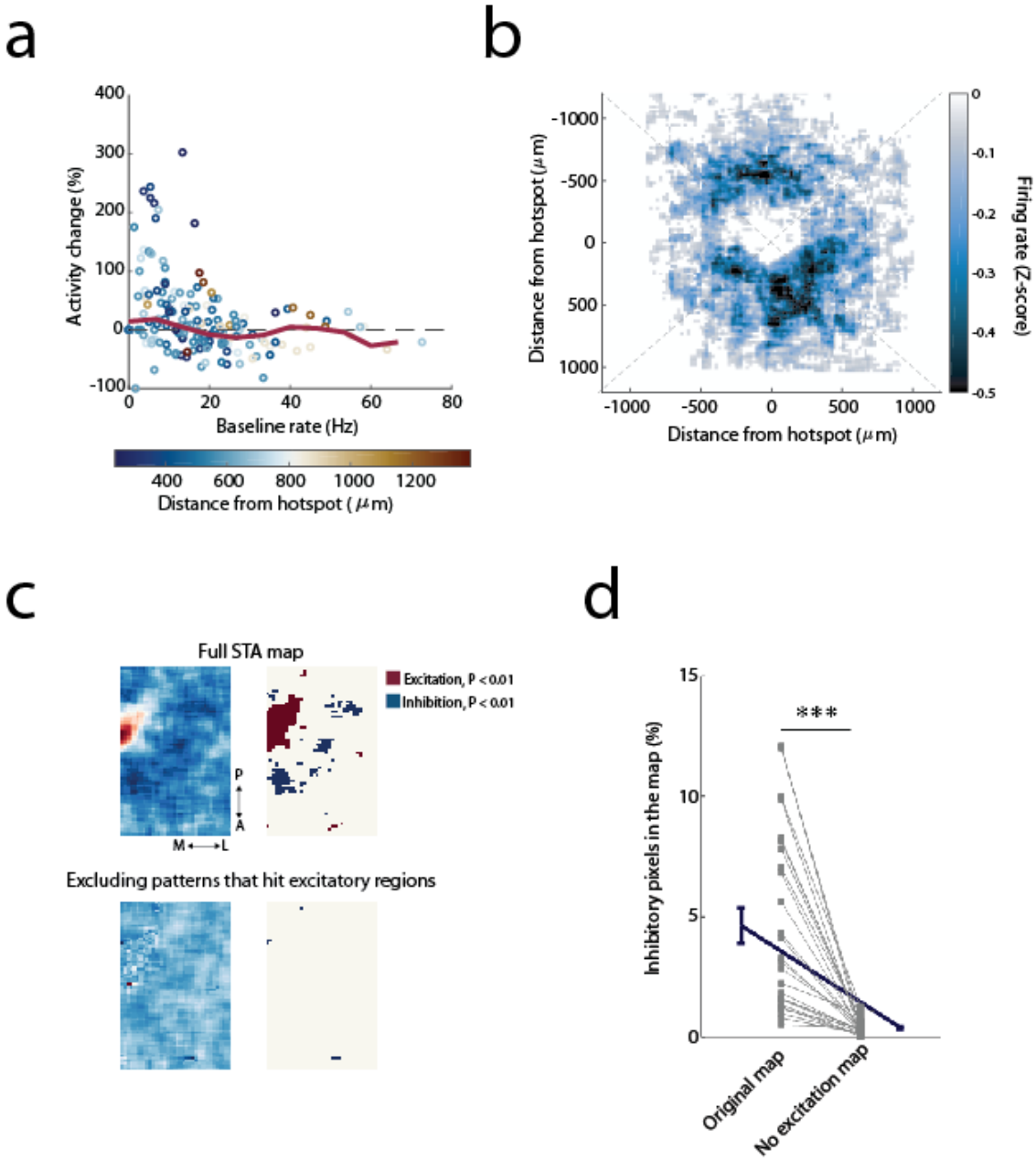

Supplementary Figure 2: MTC lateral suppression is activity- and spatially-dependent

a) Light stimulating a lateral spot without stimulating the hotspot has no effect on the recorded neuron's baseline firing rate, regardless of its firing rates. Color code as in **Figure 2d**.
b) Lateral inhibition is confined in space. All STA maps were centered at the hotspot location (N = 27 Z-scored maps, see Methods).
c) MTC lateral suppression is effective only when the target MTC is activated. Upper panels: an example of an MTC STA map and the corresponding significance map.

Lower panels: the same maps recomputed by excluding all light patterns that stimulated the region around the hotspot (All pixels with significant excitation P < 0.01, relative to shuffled data). No inhibitory regions are detected after exclusion.

d) Population analysis across all MTC STA maps (N = 27) of the percent of inhibitory pixels in the original STA map and when we excluded the light patterns that hit the hotspot area. A pixel is defined as inhibitory if its value is below two standard deviations from the shuffled distribution (see Methods). The percent of inhibitory pixels drops considerably (P = 1.8e-6, two-tailed paired *t*-test), in the excitation-excluded map.

Two different neural circuits mediate spike suppression and entrainment

In our experimental design, the same MTC participated in more than one pairing. Analyzing these pairs revealed that while light-stimulation of one pair could enhance the spike-precision without affecting its firing rate, activation of a different pair at the same light intensity could suppress the MTC firing rate without affecting its spike-precision (Figure 3a). Furthermore, light-activating the same pair with two different intensities could suppress the MTC firing rate at one intensity and enhance spike entrainment in the second (Figure 3b). These findings strongly suggest that spike suppression and entrainment are not features of the recorded cell type (i.e., mitral versus tufted cells) but instead reflect two different circuits which the MTCs form with each other.

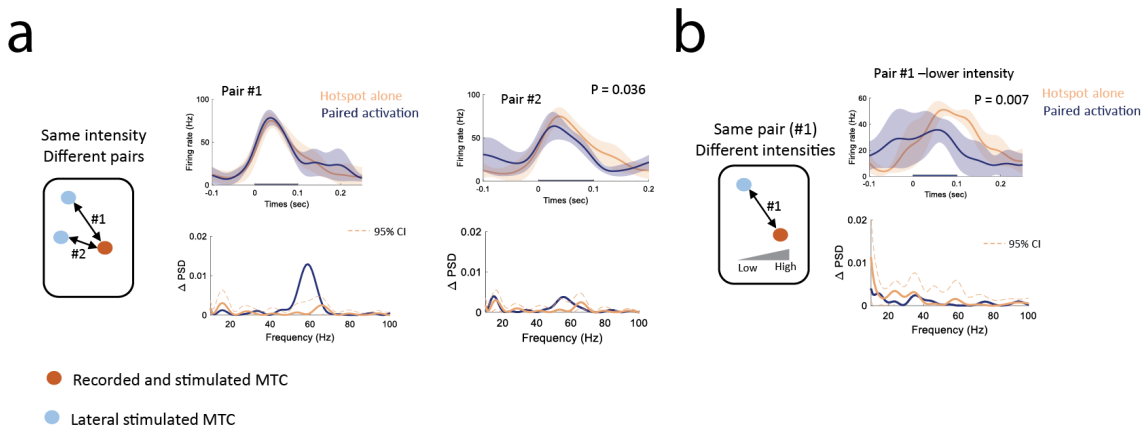

Figure 3: Spike entrainment and suppression are mediated by two different circuits

a) Light-stimulation of two different MTC pairings sharing the same postsynaptic MTC. Light-activating pair #1 (left) caused potent entrainment (P < 0.05, two-sample bootstrap) without affecting the light-evoked firing rate (P = 0.59, two-tailed paired *t*-test), whereas light-activating pair #2 (right) suppressed the MTC firing rate (P = 0.036,

two-tailed paired *t*-test), without affecting the spikes precision (P > 0.05, two-sample bootstrap).

b) Two different light intensities were applied to pair #1, which had differential effects on suppression and entrainment. High light intensity increased spike entrainment without affecting the firing rate (left panel in **a**). In contrast, lower intensity reduced the light-evoked firing rate (P = 0.007, two-tailed paired *t*-test), with no effect on the spikes' gamma entrainment (P > 0.05, two-sample bootstrap).

GC activation increases MTC synchrony in an activity-dependent and location-independent manner

We next sought to understand the neural circuits that mediate spike entrainment and suppression. We examined whether GC-MTC interactions underlie the temporal changes or the suppressive interactions we found. We conditionally expressed ChR2 in GCs by injecting AAV5-EF1a-DIO-ChR2 to Gad2-Cre mice into the GC layer (Figure 4a) as in (Dalal and Haddad, 2022; Fukunaga et al., 2014). We used odor stimuli to activate the recorded MTC. To activate all GCs belonging to a glomerulus column we used a relatively large light spot sized ~330 μm^2 (Egger and Urban, 2006). We then tested how light-activation of subsets of GCs at different locations affects MTC odor-evoked temporal dynamics and spike rate suppression (Figure 4b; N = 4 mice, N = 31 cell-odor pairs from 22 cells). To examine the temporal effects, for each cell-odor pair we extracted the MTC odor-evoked spike phases from within the LFP-gamma cycles across all trials. We then quantified the level of spike LFP-gamma coupling using the pairwise phase consistency measure (PPC1). This measure serves to minimize the bias of the neuron's firing rate on the synchrony level (Vinck et al., 2012). Only MTCs that responded to odor by excitation were analyzed (N = 18/31, P < 0.05, two-tailed paired *t*-test). We found that light-activating GC columns significantly increased MTC spike phase-locking (Figure 4c, N = 3 light spots for each cell-odor pair, a total of 54 light spots tested, P = 0.0016, two-tailed paired *t*-test). Furthermore, the increased phase-locking depended on the level of the MTC firing rate and did not significantly correlate with the distance from the MTC (Figure 4d-e). Plotting the odor-evoked spikes by aligning them to an arbitrary spike in each trial as in (Fukunaga et al., 2014) further showed that GC activation increased the recorded MTC spikes' gamma entrainment (Figure 4f-g). Our results strongly suggest that MTC-to-MTC lateral entrainment is mediated by spatially-distributed GCs.

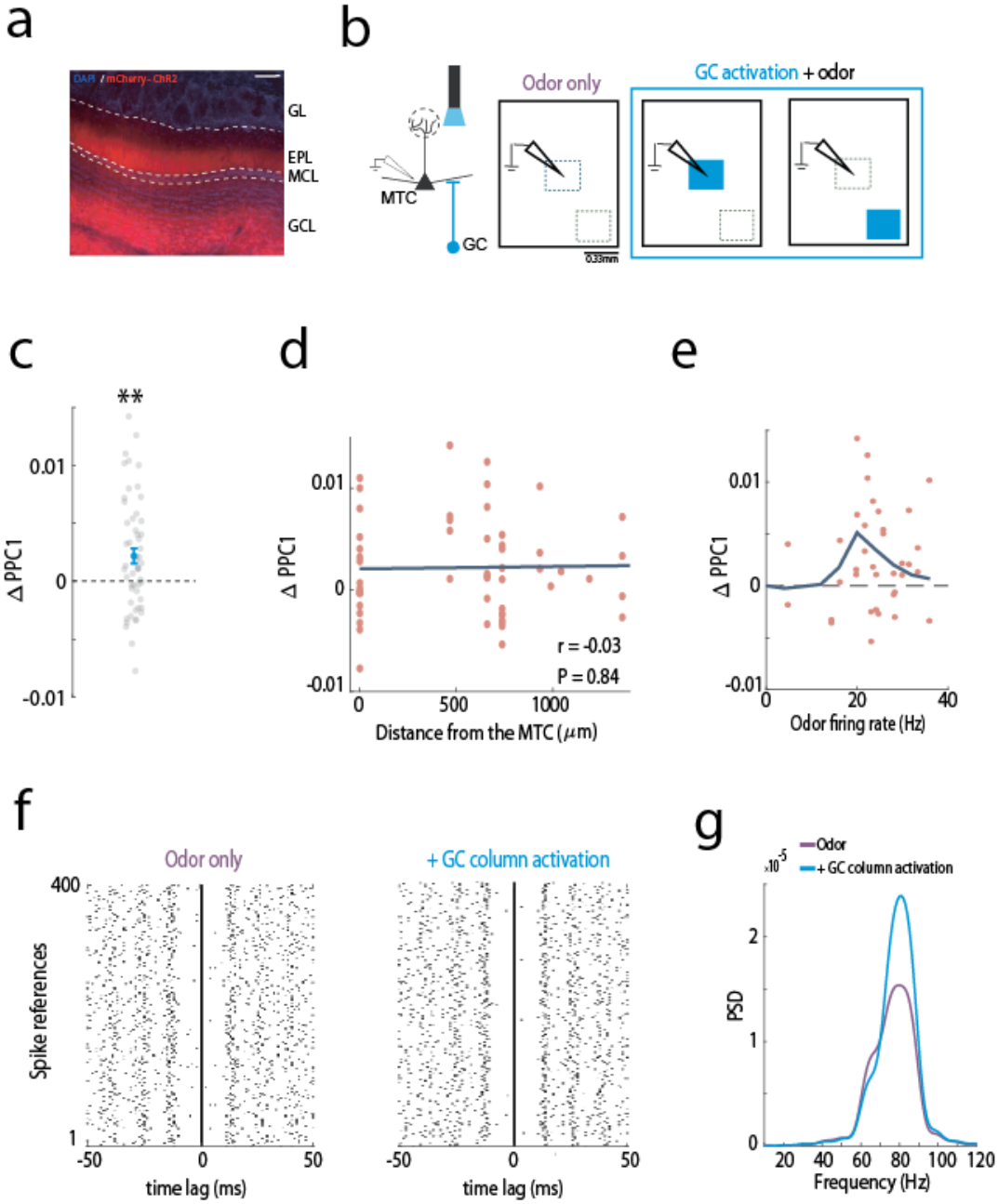

Figure 4: GC activation increases MTC synchrony in an activity-dependent and location-independent manner

a) Cre-dependent AAV injected into the GC layer (GCL) of Gad2-Cre mice. A representative example showing restricted ChR2 expression in the GCL and the external plexiform layer (EPL), into which GCs extend dendrites (red, mCherry-ChR2; blue, DAPI). MCL, mitral cell layer; GL, glomerular layer. Scale bar, 0.1 mm.

b) Schematic illustrations of the experimental setup. Left: Three weeks post injection, MTCs were recorded while light-activating subsets of GCs. Right: MTC activity was recorded in response to odor stimulation alone (purple) or combined with light-

activation of GC columns near the recording electrode or distant from it (blue). Scale bar, 330µm.

c) MTC spike synchrony to the gamma oscillation (ΔPPC1) significantly increases when we light-stimulated columns of GCs compared to odor-only stimulation (N = 54, P = 0.0016, two-tailed paired *t*-test). Only cell-odor pairs that were significantly odor-excited were analyzed (N = 18/31 cell-odor pairs; three spots were stimulated per cell odor-pair).

d) MTC spike entrainment does not depend on the GC location. The relation between the change in PPC1 caused by odor and GC stimulation as a function of the distance of the light-stimulated spot from the recording electrode. No significant correlation was found (N = 54 values from 18 cell-odor pairs, r = -0.03, P = 0. 84, Spearman correlation). Zero denotes the spot above the recording electrode.

e) MTC spike entrainment is activity-dependent. The change in synchrony peaked when MTCs fired at ~25Hz.

f) Odor-evoked spike reference analysis. Two spike raster plots are shown, for odor only (left, purple), and odor with light-activation of a GC column (right, blue). In each raster plot, spikes are plotted relative to a randomly chosen spike during the odor presentation period (N = 400 spikes references, see Methods). Note, the potent spike entrainment when GCs are activated. This analysis was performed on a cell that had a sufficiently high firing rate. This cell is likely a tufted cell due to its potent entrainment at the high gamma range, as shown in (Burton and Urban, 2021; Fukunaga et al., 2014).

g) The power spectral densities (PSD) for the two conditions in **f**. A multi-taper analysis of the circular convolution of each spike raster plot was used to compute the PSD (see Methods).

MTC suppression is not mediated by Granule cells

Finally, we examined how GC activation affects MTC odor-evoked firing rate using the same data from the previous experiment (Figure 4). We found that light-activating sets of GCs did not change the mean MTC odor-evoked firing rates, irrespective of the MTC firing rate levels. (Figure 5a; N = 54 light spots tested from 18 cell-odor pairs, P = 0.64, two-tailed paired *t*-test). Moreover, the lack of activity change did not depend on the distance of the activated GCs from the recorded MTC (Figure 5b; proximal GCs: N = 18, slope = 1, P = 0.69; distal GCs: N = 36, slope = 0.99, P = 0.69, two-tailed paired *t*-test). These findings suggest that GCs are unlikely to underlie the activity-dependent suppression we observed between MTCs (Figure 2). To conclude, our results strongly suggest that MTC-to-MTC lateral entrainment is mediated by spatially distributed GCs, while lateral-suppression, occurring most strongly between adjacent MTCs, is not mediated by GCs.

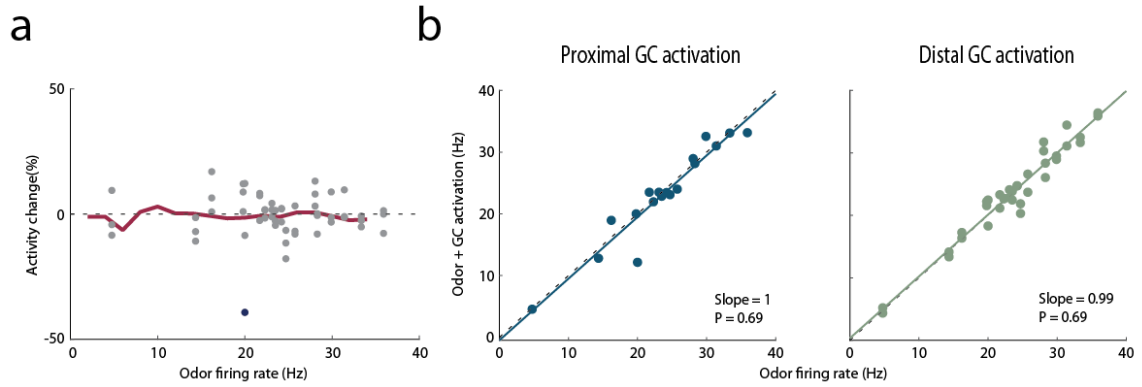

Figure 5: MTC-to-MTC firing rate suppression is not mediated by GCs

a) MTC-to-MTC lateral suppression is not mediated by GCs. Similar to Figure **2d**, the change in odor-evoked activity following GC activation is plotted as a function of the recorded MTC odor-evoked firing rates. Filled blue circles denote significant activity change ($P < 0.05$, two-tailed unpaired *t*-test). A moving average is shown in red.

b) Odor-evoked firing rates are not suppressed when a GC column is activated, irrespective of the odor-evoked MTC firing rate. Two plots are shown for activation of proximal (i.e., in the electrode vicinity, N = 18, blue) and distal GCs (all other locations, N = 36, green). The slopes of a linear fit and their P-values are plotted in each panel.

Discussion

Our findings demonstrate two types of interactions between MTCs that shape their firing rate and temporal dynamics. These two interactions are spatially-dissociated: Lateral entrainment spans the whole accessible bulb surface, while lateral suppression tends to occur primarily between MTCs, activated by adjacent glomeruli. Interestingly, both interactions are activity-dependent, with lateral entrainment and lateral suppression peaking when the postsynaptic MTC fires at ~40Hz and ~70-80Hz, respectively. Furthermore, we found that, in contrast to previous reports, GCs do not mediate MTC-MTC lateral suppression.

MTC and GC interactions facilitate the synchronizing of co-active and spatially-dispersed MTCs

It has been shown that two active MTCs can synchronize their odor-evoked spike timing (Kashiwadani et al., 1999; Schoppa, 2006). However, how this is achieved and how only

372 the odor-activated MTCs are synchronized is unknown. A recent study hypothesized that
373 GCs may support the synchronizing of odor-responding MTCs (Egger and Kuner, 2021).
374 This hypothesis postulates that the spikes of all strongly co-activated MTCs are
375 synchronized to the gamma rhythm, presumably through the GC network. Consistent with
376 this hypothesis, here we have shown that activation of one group of MTCs can increase the
377 synchrony of other, distant, active MTCs, regardless of the distance between them. Most
378 interestingly, we found that this increase in synchronization occurred only if the
379 postsynaptic MTC was firing at a certain level (Figure 1), suggesting a simple mechanism
380 by which odor-activated MTCs are synchronized. Furthermore, as predicted, we show that
381 GCs are the interneurons that enable this synchronization.
382
383 **Lateral suppression is restricted to adjacent and active MTCs**
384 In contrast to the lateral entrainment interactions, we found lateral suppression of MTC
385 spiking is effective mostly between adjacent MTCs and when the postsynaptic neuron is
386 active at a specific range (~30-80Hz, Figure 2). However, even when these conditions are
387 met, only ~20% of the tested MTC pairs exhibited significant lateral inhibition. This rate
388 is consistent with previous *in-vitro* studies that found lateral suppression between 10-20%
389 of heterotypic MTC pairs (Isaacson and Strowbridge, 1998; Urban and Sakmann, 2002).
390 These results are also consistent with the increasing evidence that MTC-to-MTC
391 suppression is relatively sparse (Fantana et al., 2008; Lehmann et al., 2016; Pressler and
392 Strowbridge, 2017). The role of this sparse inhibition is unclear. One study suggested that
393 activity-dependent lateral suppression can sharpen MTC odor responses by contrast
394 enhancement (Arevian et al., 2008). However, a direct experimental evidence is still
395 lacking.
396
397 **GCs do not substantially affect MTC odor-evoked responses.**
398 GCs are the most abundant interneuron type in the OB (Shepherd, 1972), suggesting GCs
399 have a key role in regulating MTC activity. In line with this hypothesis, several key studies
400 have provided evidence that GCs may suppress the MTC firing rate (Arevian et al., 2008;
401 Giridhar et al., 2011; Yokoi et al., 1995). Here, we show that optogenetically activating
402 arbitrary GC-columns during odor stimulation did not substantially affect MTC odor-

403 evoked firing rates. Although this contradicts several previous in-vitro results, it is
404 consistent with a recent in-vivo study that found no increase in MTC odor-evoked firing
405 rates when silencing GC activity either in anesthetized or in awake mice (Fukunaga et al.,
406 2014). It is worth noting that light-activating large numbers of GCs can suppress MTC
407 odor-evoked responses (Dalal and Haddad, 2022; Gschwend et al., 2015). However,
408 activation such as this is unlikely to occur during natural odor response. We speculate that
409 MTC-to-MTC suppression is mediated by EPL interneurons, most likely the Parvalbumin
410 neuron (PV) (Burton, 2017; Kato et al., 2013; Miyamichi et al., 2013). Future studies are
411 required to shed light on how PV neurons affect MTC activity.
412

413 **Downstream integration of synchronous MTC activity**

414 How do downstream olfactory cortex neurons benefit from synchronous MTC activity?
415 Anterior piriform cortex (aPC) neurons integrate the activity of several active MTCs and
416 act as coincidence detectors (Davison and Ehlers, 2011; Haddad et al., 2013). Recently, we
417 have shown that increased MTC spike phase-locking to OB gamma oscillations enhanced
418 aPC neurons' odor representation (Dalal and Haddad, 2022). This current study extends
419 these findings as it demonstrates that the co-activation of MTCs increases their spikes'
420 gamma entrainment. Moreover, this lateral synchronization is mediated via the GC
421 network. In summary, we found that MTC interactions shape odor-evoked MTC firing
422 rates and spike times. Both of these changes are activity-dependent. Activity-dependent
423 synchronization enables the synchronization of odor-activated MTCs that are dispersed on
424 the OB surface. Such a mechanism is likely to enhance odor information transmission to
425 downstream neurons. On the other hand, activity-dependent spike suppression might
426 enhance odor representation in the OB by reducing low and noisy MTC responses. Finally,
427 our findings suggest that two different OB interneurons mediate these distinct interactions.

428 **Acknowledgments**

429 This study was supported by a grant from the Israel Science Foundation ICORE program
430 [11/51].
431 **Author Contributions:** T.D. performed the experiments and analyzed the data, T.D. and
432 R.H conceptualized the experiments and wrote the paper.

433 **Competing Interest Statement:** The authors declare no conflict of interest.

434 **Methods**

435 All surgical and experimental procedures were conducted in accordance with the
436 National Institutes of Health Guide for the Care and Use of Laboratory Animals and Bar
437 Ilan University guidelines for the use and care of laboratory animals in research, and
438 were approved and supervised by the Institutional Animal Care and Use Committee
439 (IACUC). Animals were housed in a group cage and received no experimental treatment,
440 except genotyping. The animals were maintained in a reverse light/dark cycle, and all
441 experiments were performed during the dark period. 19 Tbet-Cre (Jackson Laboratory,
442 Stock No. 024507) crossed with Ai32 (Jackson Laboratory, Stock No. 012569), and 4
443 Gad2-ires-Cre (Jackson Laboratory, Stock No. 028867) male and female mice aged 3-12
444 months were used. As no differences in light-evoked responses were observed between
445 sexes, data from both sexes was pooled.

446

447 **Surgical Procedures for Electrophysiology Recordings**

448 Animals were anesthetized with ketamine/ medetomidine (60/ 0.5 mg/ kg, i.p.) and then
449 fixed in a stereotaxic frame. The bone overlaying the dorsal OBs was removed. Additional
450 anesthesia was administered as needed (~30% of the original dose of ketamine/
451 medetomidine). Body temperature was maintained at 36-37°C using a homoeothermic
452 blanket system (Harvard Apparatus).

453

454 **Viral Injections**

455 Mice were briefly anesthetized with isoflurane before intraperitoneal injection of ketamine/
456 medetomidine (60/ 0.5 mg/ kg i.p.). The mouse was head-fixed in a stereotaxic frame, and
457 AAV5-EF1a-DIO-ChR2-eYFP/mCherry (titers: $4x10^{12}$ particles/ ml; University of North
458 Carolina Gene Therapy Center) was injected into the granule cell layer. To infect GCs in
459 the GCL, we modified an injection protocol employing five injection sites in two tracks,
460 as reported elsewhere (Fukunaga et al., 2014). The coordinates for the first track were +0.9
461 mm (M-L) from the midline rhinal fissure, +0.8 mm (A-P), and three sites at the D-V axis
462 at -0.8 mm (300 nl), -1.1 mm (200 nl), and -1.3 mm (200 nl). Second track coordinates
463 were +0.9 mm (M-L) from the midline rhinal fissure, +1.2 mm (A-P) and 2 sites at the D-
464 V axis at -0.8 mm (200 nl), and -1.1 mm (200 nl). M-L coordinates are relative to the

465 midline rhinal fissure. The syringe was left in place for at least three minutes before moving
466 to the next coordinate on the D-V axis. Electrophysiology was carried out at least three
467 weeks post-viral injection. The virus was injected using a micro-injector (IMS-10,
468 Narishige, Japan) at a rate of 70 nl/ min, which was left in place for 5 minutes to allow
469 viral particle diffusion before needle removal. Incisions were closed with tissue glue
470 (Vetbond), and an analgesic injection (Carprofen) was administered at the end of the
471 surgery.
472
473 **Electrophysiology**
474 The neurons' extracellular activity and local-field potential (LFP) were recorded using
475 tungsten electrodes (~1-10 MΩ; FHC). Neural signals were amplified and first filtered at
476 1-10,000Hz and then at 300-5,000 Hz for spiking activity (AM-Systems 1800), sampled,
477 and recorded at 40 kHz (National Instruments, Austin, TX). Spike signals were sorted
478 offline using MClust software in MATLAB (written by A.D. Redish, University of
479 Minnesota). MTC recordings were collected from the dorsal OB (~200-500 μm). The
480 electrode was typically lowered at an angle of 90 degrees. The depth of recorded neurons
481 was estimated when the recording electrode was withdrawn using a micromanipulator.
482
483 **Optogenetic Stimulation of the Olfactory Bulb**
484 Optogenetic stimulation of neurons in the OB was performed using an optical imaging
485 system based on a digital micro-mirror (OPTOMA X600 DLP Projector), as described
486 (Grobman et al., 2018). Precise spatial control of optical stimulation was achieved by
487 projecting two-dimensional light patterns over the dorsal surface of the OB. We used blue
488 and white light for MTC and GC activation, respectively. For MTC stimulation (Tbet-Cre
489 mice crossed with Ai32 mice), a blue filter was placed on top of the collimating lens, which
490 was placed at a distance of ~20 cm from the projector (f = 75 mm, Achromatic doublets,
491 Thorlabs). This configuration resulted in an image where each projected pixel
492 corresponded to a square of 22 μm^2. The size of the craniotomy determined the light
493 stimulation boundaries of each experiment. Optical stimulation was controlled with the
494 MATLAB psychophysical toolbox. We used a photodiode (FDS1010, 400-ns rise time,
495 Thorlabs) to obtain a timestamp for each light stimulus. The light intensity ranged between

496 ~0.1-~1.5 mW/ mm^2 as measured with an optical power meter (Thorlabs PM100D). The
497 stimulation frequency of the optical imaging system was 120 Hz.
498
499 **Spike-Triggered Average (STA)**
500 The spike-triggered average calculation was described previously by (Grobman et al.,
501 2018). Briefly, STA was used to characterize the receptive field of the recorded MTC.
502 Here, we use the term 'receptive field' in a more abstract sense to refer to the ensemble of
503 all neurons on the bulb's surface that modify the recorded neuron activity.
504 We stimulated the dorsal OB with patterns of multiple square spots measuring 88-110 μm^2.
505 Light spots within a pattern could overlap up to a shift of one pixel (22μm). The stimuli
506 duration was 0.1 sec, and the inter-stimuli-interval between consecutive patterns ranged
507 between 0.1-0.2 sec. The number of spots projected in each trial ranged between 5-10, and
508 the number of trials per recorded ranged between 2000-3000. We computed the response
509 map for each cell by computing the spike-triggered average, which is the weighted firing
510 rate average of all projected stimuli.

511 $$STA = \frac{\sum_{i=1}^{N} P_i R_i}{\sum_{i=1}^{N} R_i}$$

512 P_i is the 2-dimensional projected light pattern, and R_i is the evoked firing rate following
513 stimulus P_i.
514
515 **Paired light stimulation**
516 Single light spots (over the hotspot or a lateral spot) or paired stimulation (both together)
517 of size ~154 μm^2 were projected at varying light intensities (range ~0.1 to ~1.5 mW/ mm^2,
518 reported in Figures 1-3). The lateral spots were selected based on the STA map or
519 randomly. The number of trials for each condition at a given light intensity was 15, and the
520 inter-stimuli-interval (ISI) was set to 1.5 seconds.
521
522 **Optogenetic activation of GCs during baseline and odor stimulation**
523 To verify the effect of optogenetic activation of GCs on the recorded MTC, we scanned
524 the OB with light spots, without stimulating the MTC. Light spots were of size 330μm^2,
525 each spot was illuminated 20-30 times, the light duration was 0.2 sec, and the ISI was 0.4

526 sec. The light intensity was as described in (Dalal & Haddad 2022). As expected, we found
527 a 'coldspot' (i.e. a reduction in firing rate) in the vicinity of the electrode location (data not
528 shown), confirming that light-activating GCs evokes enough inhibition to reduce MTC
529 baseline activity, consistent with a recent study (Huang et al., 2016). For optogenetic
530 activation of GCs during odor stimulation, the odor duration was 1.5 seconds. The light
531 stimulus was active throughout the entirety of the odor stimulation period. The activation
532 of proximal and distal GCs during odor stimulation was performed based on the activity
533 map generated under baseline conditions. In each of the three conditions in this experiment,
534 odor stimulation alone or combined with local or lateral GCs activation, the number of
535 trials was at least 10, with an ISI of 10-15 seconds. In these experiments, the LFP was
536 simultaneously recorded with the same electrode, and the signal was later filtered for
537 spiking activity (300-5000 Hz) and LFP ranges (1-300 Hz).
538
539 **Respiration Analysis**
540 We recorded the respiration signal using a piezoelectric sensor (APS4812B-LW100-R,
541 PUI Audio). The most salient feature of the respiratory signal is the peak in the middle of
542 the inhalation cycle caused by the pressure of the diaphragm on the sensor. The onsets of
543 inhalation and exhalation were defined as the zero-crossings of the signal before and after
544 the peak, respectively.
545
546 **Odorant Application**
547 Odorants were applied using a custom-built olfactometer. Odorants were diluted in mineral
548 oil (1:100) and stored in sealed glass vials. This concentration was chosen to elicit a
549 detectable response. The tubes were placed in front of the animals' nostrils at a distance of
550 ~2 cm. Airflow was controlled with a mass flow controller (Agilent, Alimc-2LSPM) and
551 set to 0.8 slpm. Air circulated freely between stimulations to reduce =odorant remnants. A
552 vent removed residual odorants. Odorant stimulation times and sequences were controlled
553 by custom MATLAB scripts. The odorant stimulation time was set to 1.5 sec., with an
554 inter-trial interval of 10-15 sec. The odorant sequence was randomized, and each stimulus
555 was delivered at least ten times. All odorants used (all at 1% dilution) were from Sigma-
556 Aldrich at their highest purity. The odorants used in the first experiment (reported in Figure

557 2) were Phenethylamine (PEA (CAS: 64-41-0), Ethyl acetate (CAS: 141-78-6), ethyl
558 valerate (CAS: 539-82-2), 2-heptanone (CAS: 110-43-0), ethyl butyrate (CAS: 105-54-4),
559 ethyl tiglate (CAS: 5837-78-5), and acetophenone (CAS: 98-86-2).
560
561 **QUANTIFICATION AND STATISTICAL ANALYSIS**
562 **General Statistical Analysis**
563 All data analyses were performed in MATLAB. The figures or figure legends detail the
564 number of data points used for all statistical tests and graphs. Significance alpha was
565 defined as a 0.05/0.01. Unless stated otherwise, we report the mean ± SEM or %95
566 confidence interval. Mean ± standard deviation is reported when estimated from a bootstrap
567 process. We used a *t*-test as required by the test's null hypothesis and population
568 assumptions. All tests were two-tailed. The test is reported in the figure legend or the main
569 text.
570
571 **Data Analysis**
572 **Spike Sorting**
573 Spike signals were sorted and clustered offline using MClust software in MATLAB
574 (written by A.D. Redish) or Spike3D (Neuralynx). Only visually well-isolated clusters
575 were used, with less than 5% of spikes violating an inter-spike interval of 2 ms.
576
577 **Significant regions in the STA map**
578 Computation of significant activity change of each pixel of the STA map was done relative
579 to a shuffled STA map. The shuffled map was generated by shuffling the patterns indices
580 and computing the shuffled STA (multiplying the shuffled patterns with the original firing
581 rate as described above). Then, the 0.5 and 99.5 percentile values from the shuffled map
582 were determined. The values in the STA map that were above or below these low and high
583 percentile thresholds were assigned as significant excitatory and inhibitory pixels,
584 respectively.
585
586 **Superimposed STA maps**
587 To analyze the spatial location of the inhibitory regions surrounding the recorded MTC,

each STA map was Z-scored using the mean and standard deviation values on the map. We then thresholded the map such that only pixels with a Z-score <= -1 remained. The hotspot peak was centered at the origin, and the inhibition values were plotted on the map relative to the hotspot. We superimposed all maps and averaged across all neurons.

Exclusion of excitatory regions in STA maps

STA maps were recomputed by excluding trials with at least one light spot that hit the significant excitatory regions in the map. The significance of each pixel in the recomputed map was registered, and the percent of inhibitory pixels in the original and recomputed map was assigned. To verify that the lower number of significant pixels in the recomputed map was not due to a smaller number of trials, for each full map we randomized the same number of trials that were used to construct the recomputed map and computed the STA. We found no significant change in the percent of inhibitory spots compared with the original map (data not shown).

Quantification of MTC lateral inhibition

A pair of light-stimulated MTCs was considered as evoking lateral inhibition if it met two criteria: the response to the hotspot stimulation was significantly different from baseline ($P < 0.05$, one-tailed paired *t*-test), and there was a significant change in the firing rate across trials between hotspot stimulation and paired activation within a window of 200 ms ($P < 0.05$, two-tailed unpaired *t*-test, stimulus duration 100 ms). A window of 200 ms was used to account for neural responses with a slower return to baseline. The distance between the spots in the pair was measured using Euclidean distance. The activity change measure was defined as:

$$100\,X\,\frac{mean(paired\ activation\ firing\ rate) - mean(hotspot\ firing\ rate)}{mean(hotspot\ firing\ rate)}$$

MTC entrainment across and within trials

Quantifying MTC spike entrainment across trials was done by computing the PSTH of each condition during the light period (100 ms) using a Gaussian kernel with a standard deviation of 2 ms. The PSTHs were zero-padded to a length of 1 second, Z-scored, and the

power spectrum density was computed using multi-taper analysis (TW = 3 Hz, L = (2*TW)-1, where L is the number of orthogonal Slepian tapers). The delta entrainment value was the difference between the integral of paired activation and the hotspot alone at 40-70 Hz. We analyzed only pairs and light intensities that significantly responded to light stimulation ($P < 0.05$, two-tailed paired *t*-test). Shuffled distribution of spike entrainment was obtained by shuffling the trial identities and computing the power spectrum density integral difference. Delta entrainment values were labeled significant if they crossed the 95% confidence interval around the shuffled distribution. To quantify the change in spike entrainment within trials, each trial was convolved with a Gaussian window (standard deviation of 2 ms), the power spectrum was computed per trial, and the spectrums were averaged across all trials. The delta entrainment within trials was computed as the sum of the difference between the averaged power spectrums of the two conditions.

Time-Frequency Analyses of MTC entrainment

Time-frequency representation was performed using the continuous wavelet transform (the analytic 'Morse' wavelet, 8 octaves, 32 voices per octave; MathWorks) over the Peri-stimulus time histograms (PSTH) across trials (Gaussian window of 2 ms standard deviation).

Odor-Evoked Responses

An odor firing rate was computed over the first two seconds following odor presentation. This time window included an additional 0.5 sec after stimulus offset to account for neural responses with a slower return to baseline. Trials were aligned to odor onset so that the analyzed neural activity would be aligned with the light stimulation. A response was defined as significant if the firing rate was significantly different from the average firing rate over an equivalent time window prior to stimulus onset ($P < 0.05$, two-tailed paired *t*-test). PSTHs were smoothed using a Gaussian filter (standard deviation of 50 ms, Chronux toolbox).

LFP Analysis

Recorded LFP signals were down-sampled to 4 kHz and band-pass filtered to the γ-band

649 frequency range (40-70 Hz) using the MATLAB (MathWorks) filter designer (Butterworth
650 IIR filter with order 1). The line noise (50 Hz) was filtered using an IIR bandstop filter (48-
651 52 Hz). We focused our analysis on the low γ-band frequency range as a prominent
652 oscillation in this range in the olfactory bulb was previously reported (Cenier et al., 2009;
653 Lepousez and Lledo, 2013).
654
655 **Spikes-LFP pairwise phase consistency (PPC)**
656 Spike-LFP coupling was computed using the pairwise phase consistency 1 (PPC1) measure
657 (Vinck et al., 2012, 2013). For each neuron, we extracted the spike phases from all trials.
658 To compute the spike phases per trial, we extracted the instantaneous phase of the
659 corresponding γ-band-filtered LFP (40-70 Hz) using the Hilbert transform, assigned a
660 phase to each spike (0–2π) and pooled the phases across all trials. The PPC1 values were
661 the mean dot-product of all pairwise spike phases, excluding phases of spikes from the
662 same trial.
663
664 **Spike reference analysis**
665 We performed a spike reference analysis to quantify the entrainment of odor-evoked MTC
666 spikes, as seen elsewhere (Fukunaga et al., 2014). Spike reference raster plots were
667 constructed for each condition by randomizing 400 spikes from all trials that occurred at a
668 time window of 1 second after odor onset. Each randomized spike served as a reference
669 and was set to time lag 0, and the spikes in a window of ± 50 ms around it were plotted
670 relative to the reference. Choosing a different number of randomized spikes or a different
671 window size did not affect the results. We then computed the PSTH of the raster plot,
672 subtracted its mean, and performed a circular convolution. To compute the power spectral
673 density of the raster plot, we zero-padded the convolved signal into one 1-second length
674 and applied a multi-taper analysis (TW = 5 Hz). The PSD curve was smoothed using a
675 rectangular window of order 15.
676
677
678 **<u>Bibliography</u>**
679 Arevian, A.C., Kapoor, V., and Urban, N.N. (2008). Activity-dependent gating of lateral

inhibition in the mouse olfactory bulb. Nat Neurosci *11*, 80–87.

Beshel, J., Kopell, N., and Kay, L.M. (2007). Olfactory bulb gamma oscillations are enhanced with task demands. J. Neurosci. *27*, 8358–8365.

Burton, S.D. (2017). Inhibitory circuits of the mammalian main olfactory bulb. J. Neurophysiol. *118*, 2034–2051.

Burton, S.D., and Urban, N.N. (2021). Cell and circuit origins of fast network oscillations in the mammalian main olfactory bulb. Elife *10*, 1–29.

Buzsáki, G. (2010). Neural Syntax: Cell Assemblies, Synapsembles, and Readers. Neuron *68*, 362–385.

Buzsáki, G., and Chrobak, J.J. (1995). Temporal structure in spatially organized neuronal ensembles: a role for interneuronal networks. Curr. Opin. Neurobiol. *5*, 504–510.

Cenier, T., François, D., Philippe, L., Samuel, G., Corine, A., and Nathalie, B. (2009). Respiration-gated formation of gamma and beta neural assemblies in the mammalian olfactory bulb. Eur. J. Neurosci. *29*, 921–930.

Dalal, T., and Haddad, R. (2022). Upstream γ-synchronization enhances odor processing in downstream neurons. Cell Rep. *39*, 110693.

Davison, I.G., and Ehlers, M.D. (2011). Neural circuit mechanisms for pattern detection and feature combination in olfactory cortex. Neuron *70*, 82–94.

Egger, V., and Kuner, T. (2021). Olfactory bulb granule cells: specialized to link coactive glomerular columns for percept generation and discrimination of odors. Cell Tissue Res. *383*, 495–506.

Egger, V., and Urban, N.N. (2006). Dynamic connectivity in the mitral cell-granule cell microcircuit. Semin. Cell Dev. Biol. *17*, 424–432.

Fantana, A.L., Soucy, E.R., and Meister, M. (2008). Rat olfactory bulb mitral cells receive sparse glomerular inputs. Neuron *59*, 802–814.

Fukunaga, I., Herb, J.T., Kollo, M., Boyden, E.S., and Schaefer, A.T. (2014). Independent control of gamma and theta activity by distinct interneuron networks in the olfactory bulb. Nat. Neurosci. *17*, 1208–1216.

Galán, R.F., Fourcaud-Trocmé, N., Ermentrout, G.B., and Urban, N.N. (2006). Correlation-induced synchronization of oscillations in olfactory bulb neurons. J. Neurosci. *26*, 3646–3655.

711 Giridhar, S., Doiron, B., and Urban, N.N. (2011). Timescale-dependent shaping of
712 correlation by olfactory bulb lateral inhibition. Proc Natl Acad Sci U S A *108*, 5843–
713 5848.
714 Grobman, M., Dalal, T., Lavian, H., Shmuel, R., Belelovsky, K., Xu, F., Korngreen, A.,
715 and Haddad, R. (2018). A Mirror-Symmetric Excitatory Link Coordinates Odor Maps
716 across Olfactory Bulbs and Enables Odor Perceptual Unity. Neuron *99*, 800-813.e6.
717 Gschwend, O., Abraham, N.M., Lagier, S., Begnaud, F., Rodriguez, I., and Carleton, A.
718 (2015). Neuronal pattern separation in the olfactory bulb improves odor discrimination
719 learning. Nat. Neurosci. *18*, pages1474–1482.
720 Haddad, R., Lanjuin, A., Madisen, L., Zeng, H., Murthy, V.N., and Uchida, N. (2013).
721 Olfactory cortical neurons read out a relative time code in the olfactory bulb. Nat.
722 Neurosci. *16*, 949–957.
723 Huang, X.L., Ung, K., Garcia, I., Quast, K.B., Cordiner, K., Saggau, X., and Arenkiel,
724 X.B.R. (2016). Task Learning Promotes Plasticity of Interneuron Connectivity Maps in
725 the Olfactory Bulb. *36*, 8856–8871.
726 Isaacson, J.S., and Strowbridge, B.W. (1998). Olfactory reciprocal synapses: dendritic
727 signaling in the CNS. Neuron *20*, 749–761.
728 Kashiwadani, H., Sasaki, Y.F., Uchida, N., and Mori, K. (1999). Synchronized oscillatory
729 discharges of mitral/tufted cells with different molecular receptive ranges in the rabbit
730 olfactory bulb. J. Neurophysiol. *82*, 1786–1792.
731 Kato, H.K., Gillet, S.N., Peters, A.J., Isaacson, J.S., and Komiyama, T. (2013).
732 Parvalbumin-Expressing Interneurons Linearly Control Olfactory Bulb Output. Neuron.
733 Lehmann, A., D'Errico, A., Vogel, M., and Spors, H. (2016). Spatio-Temporal
734 Characteristics of Inhibition Mapped by Optical Stimulation in Mouse Olfactory Bulb.
735 Front. Neural Circuits *10*, 15.
736 Lepousez, G., and Lledo, P.M. (2013). Odor Discrimination Requires Proper Olfactory
737 Fast Oscillations in Awake Mice. Neuron.
738 Macleod, K., Laurent, G., and Ba, A. (1998). Who reads temrpoal information contained
739 across synchonized and oscillatory spike trains? Nature *395*, 693–698.
740 Miyamichi, K., Shlomai-Fuchs, Y., Shu, M., Weissbourd, B.C., Luo, L., and Mizrahi, A.
741 (2013). Dissecting local circuits: Parvalbumin interneurons underlie broad feedback

control of olfactory bulb output. Neuron *80*, 1232–1245.

Pressler, R.T., and Strowbridge, B.W. (2017). Direct Recording of Dendrodendritic Excitation in the Olfactory Bulb : Divergent Properties of Local and External Glutamatergic Inputs Govern Synaptic Integration in Granule Cells. *37*, 11774–11788.

Pritchett, D.L., Siegle, J.H., Deister, C.A., and Moore, C.I. (2015). For things needing your attention: The role of neocortical gamma in sensory perception. Curr. Opin. Neurobiol. *31*, 254–263.

Schoppa, N.E. (2006). Synchronization of olfactory bulb mitral cells by precisely timed inhibitory inputs. Neuron *49*, 271–283.

Shepherd, G.M. (2004). The synaptic organization of the brain (Oxford University Press).

Sohal, V.S. (2016). How close are we to understanding what (If anything) γ oscillations do in cortical circuits? J. Neurosci. *36*, 10489–10495.

Urban, N.N., and Sakmann, B. (2002). Reciprocal intraglomerular excitation and intra- and interglomerular lateral inhibition between mouse olfactory bulb mitral cells. J. Physiol. *542*, 355–367.

Vinck, M., Battaglia, F.P., Womelsdorf, T., and Pennartz, C. (2012). Improved measures of phase-coupling between spikes and the Local Field Potential. J. Comput. Neurosci. *33*, 53–75.

Vinck, M., Womelsdorf, T., Buffalo, E.A., Desimone, R., and Fries, P. (2013). Article Attentional Modulation of Cell-Class-Specific Gamma-Band Synchronization in Awake Monkey Area V4. 1077–1089.

Yokoi, M., Mori, K., and Nakanishi, S. (1995). Refinement of odor molecule tuning by dendrodendritic synaptic inhibition in the olfactory bulb. Proc Natl Acad Sci U S A *92*, 3371–3375.